*Clays and Clay Minerals*, Vol. 41, No. 3, 305–316, 1993.

# THE SURFACE COULOMB ENERGY AND PROTON COULOMB POTENTIALS OF PYROPHYLLITE {010}, {110}, {100}, and {130} EDGES

WILLIAM F. BLEAM, GEREON J. WELHOUSE, AND MARK A. JANOWIAK

Department of Soil Science, 1525 Observatory Drive, University of Wisconsin–Madison
Madison, Wisconsin 53706-1299

**Abstract**—This paper describes structural models of four pyrophyllite edge faces: {010}, {110}, {100}, and {130}. Water molecules chemisorbed to Lewis acid sites stabilize edge faces both crystallochemically and electrostatically. The detailed assignment of protons to surface oxygens and the orientation of OH bond-vectors both influence the surface Coulomb energy.

The geometry chosen for the electrostatic calculations was infinite pyrophyllite ribbon the thickness of a single phyllosilicate layer and the width of 50 to 70 unit cells. Such a phyllosilicate ribbon has only two edges, a top and bottom, which were simulated using the edge-face models mentioned above. About 94% of the surface Coulomb energy is confined to the edge-face repeat unit. The surface Coulomb energies of the four edge faces are on the order of 2–3 nJ/m, varying ±1 nJ/m with proton assignment. The Coulomb potential, measured either within the layer or parallel to the layer, has a distinct negative trend near the edge face that can be traced to chemisorbed water molecules. Finally, the correlation between proton Coulomb potentials at the edge face and the coordination environment of the protons is poor, obscured by long-range interactions.

**Key Words**—Edge structure, Electrostatic potential, Lattice sum, Pyrophyllite.

## INTRODUCTION

The stability of colloidal clay mineral suspensions is believed to come from edge-to-face and edge-to-edge associations between individual clay mineral platelets (Schofield and Samson, 1953, 1954; Swartzen-Allen and Matijevic, 1974; van Olphen, 1977). Secor and Radke (1985) recently examined these associations by modeling the diffuse double-layer surrounding thin, disk-shaped particles. Two other important properties of phyllosilicates, pH-dependent surface charge and anion exchange capacity, both arise from reactions at edge faces (Schofield and Samson, 1953; Quirk, 1960; Ferris and Jepson, 1975). This paper investigates the atomic-level structure and electrostatic properties of pyrophyllite edge faces. Pyrophyllite was selected because it is a phyllosilicate whose structure and composition permit a simplified analysis of these properties, yet it bears sufficient similarities to smectites, micas, and other phyllosilicates to allow extension of this analysis to a much broader range of minerals.

Schofield and Samson (1953) describe perhaps the earliest model of a clay mineral edge face. Their model (Figure 1A) illustrated hydrolysis of three types of oxygens at a general kaolinite edge face: oxygens in the basal plane of the tetrahedral sheet bonded to Si only; oxygens in the apical plane of the tetrahedral sheet bonded to both Al and Si; and oxygens bonded to Al only. Throughout this paper these will be called basal-$O_b$, apical-$O_a$, and hydroxyl-$O_h$ oxygens, respectively.

Grim and Guven (1978) adopted the periodic-bond-chain (PBC) theory of Hartman and Perdok (1955a, 1955b, 1955c) to explain the crystal habit of phyllosilicates. Though their insights have proved valuable in later studies of edge faces, they did not propose explicit edge-face models. We will see that Grim and Guven (1978) overlooked two important PBCs.

The next major contribution is from van Santen (1982), who estimated the Madelung potential (i.e., Coulomb energy) of basal and apical oxygens and protons at a smectite edge face. These calculations require detailed, atomic-level models of the edge-face structure. Unfortunately, van Santen neither provides details of the model (e.g., bond lengths, bond angles, etc.) that would allow independent evaluation nor identifies which crystallographic edge face is represented by the model.

White and Zelazny (1988) can be credited with the most exhaustive crystallochemical study of phyllosilicate edge faces. Their A-chain model (Figure 2A) is an elaboration of the Schofield-Samson model (Figure 1A) and closely resembles that of van Santen (1982). The B-chain (Figure 2B) shares characteristics with a structure (Figure 1B) that White and Zelazny (1988) generously attribute to Muljadi *et al.* (1966). The A- and B-chain models are derived from PBCs (Hartman and Perdok, 1955a, 1955b, 1955c) that run parallel to the [110] and [100] directions, respectively, in phyllosilicates (Grim and Guven, 1978; Hartman, 1982). The C-chain (not pictured here) is equivalent by symmetry to the A-chain.

One way to evaluate the edge-face models of White and Zelazny (1988) is to consider whether they provide sufficient detail to compute the electrostatic properties of edge faces, i.e., whether it is possible to determine the coordinates of the atoms at the edge face bounded


Figure 1. Schematic models of reactive groups at the edge face of kaolinite: A) Schofield and Samson (1953) and B) Muljadi *et al.* (1966).

by the A- and B-chains. We must assume all atoms at the edge face remain in the same relative positions as in the bulk layer. Even with this assumption, the orientation of OH bond-vectors at the edge face are undetermined.

Well-crystallized phyllosilicates display a hexagonal crystal habit. The edge faces most commonly assigned to these hexagonal crystals are the {010} and the {110} (Grim and Guven, 1978; Hartman, 1982). Sun and Baronnet (1989a, 1989b) reported hexagonal phlogopite crystals whose optical axes indicated the presence of {100} and {130} edge faces.

The objective of the present study was an analysis of the electrostatic properties of phyllosilicate edge faces. Two approaches present themselves: the phenomenological approach treats the phyllosilicate layer and edge face as structureless media for which distinctions among crystallographic planes are irrelevant; the atomistic approach computes the Coulomb potentials from detailed structural models.

The current paper describes structural models, the repeat unit contents, and bond-cutting energies of four pyrophyllite edge faces: {010}, {110}, {100}, and {130}. It also provides a crystallochemical rationale for those structural models and describes a method for assigning the coordinates to all atoms at the edge face, including protons. Finally, this paper describes several computed electrostatic properties of phyllosilicate edge faces: surface Coulomb energy, the Coulomb potentials of edge-site protons and oxygens, and the distance over which phyllosilicate layers are perturbed by an edge face.

## CRYSTALLOCHEMICAL EDGE-FACE MODELS

### *Background*

White and Zelazny (1988) used PBC theory (Hartman and Perdok, 1955a, 1955b, 1955c, Hartman, 1982) to justify which bonds are cut to form a particular edge face. Ziolkowski (1986) describes a much simpler method that yields identical results: "[T]he [surface] model [is] constructed by cutting the crystal along the considered crystallographic plane in such a way as to break the weakest bonds, to retain the configuration of atoms and bond lengths characteristic for the bulk, and to conserve the stoichiometric composition."

The weakest bonds are those that take the least energy to break. A good estimate of bond energies can be made by employing the proportionality (Eq. 1) between bond valences and equivalent bond enthalpy E (O'Keeffe and Stuart, 1983; Ziolkowski and Dziembaj, 1985).

$$E = Js \quad (1)$$

Though it is simple to evaluate the energy of different cuts and arrive at a model meeting the requirements specified by Ziolkowski (1986), such an edge face is unlikely to exist in the presence of water.

Cutting of a polar solid leaves cations and anions at the cut with a lower coordination number than equivalent atoms in the bulk. These undercoordinated cations and anions are Lewis acid and base sites (van Santen, 1982; Schindler and Stumm, 1987) that are unstable in the presence of water (Schindler and Stumm,

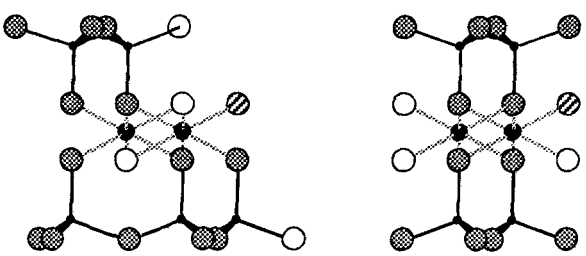


Figure 2. Profile of two 2:1 phyllosilicate edge faces adapted from White and Zelazny (1988). The edge face is on the right-hand side in each illustration with the phyllosilicate layer extending to the left. The A-chain (Figure 2A) runs parallel to the [110] crystallographic direction and borders the {110} edge face. The B-chain (Figure 2B) runs parallel to the [100] crystallographic direction and borders the {010} edge face. Shaded circles denote oxygens, open circles are hydroxyls, striped circles are water molecules, and small filled circles are aluminum atoms.

https://doi.org/10.1346/CCMN.1993.0410305 Published online by Cambridge University Press

Table 1A. Cartesian atomic coordinates for idealized pyrophyllite: $d$(Si-O) = 1.625 Angstroms; $d$(Al-O) = 1.909 Angstroms; $d$(H-O) = 0.864 Angstroms; $d$(O-O) = $(8/3)^{1/2}$ $d$(Si-O). The layer group $c2/m$ forms a rectangular lattice with basis {***a***, ***b***}. Tetrahedra are rotated $\alpha = 10°$ and the hydroxyl is inclined $\rho_{HO} = 23.1°$ from the (001). Atomic coordinates are in Angstrom units.

| $a = 2d$(O-O) cos$\alpha$ = 5.227 Angstroms; $b = (3)^{1/2}a$ = 9.053 Angstroms | | | |
|---|---|---|---|
| Atom | x | y | z |
| Al | 0.000 | 1.509[6] | 0.000 |
| $O_{apical}$ | 1.742[1] | 1.509 | 0.7804[8] |
| $O_{hydroxyl}$ | −0.8711[2] | 0.000 | 0.7804 |
| H | −1.666[3] | 0.000 | 1.119[9] |
| Si | 1.742 | 1.509 | 2.405[10] |
| $O'_{basal}$ | 2.008[4] | 0.000 | 2.947[11] |
| $O_{basal}$ | 0.3025[5] | 2.033[7] | 2.947 |

[1] {$a/3$}; [2] {$-a/6$}; [3] {[$-a/6$] − [$d$(H-O) cos$\rho_{HO}$]}; [4] {[$a/3$] + [$(1/3)^{1/2}$ $d$(O-O) sin$\alpha$]}; [5] {[$a/12$] − [$(1/12)^{1/2}$ $d$(O-O)sin$\alpha$]}; [6] {$b/6$}; [7] {[$b/4$] − [(1/2) $d$(O-O) sin$\alpha$]}; [8] $y_{O(a/h)} = \{[d(\text{Al-O})]^2 - [(32/27)^{1/2}\, d(\text{Si-O})\cos\alpha]^2\}^{1/2}$; [9] {$y_{O(a/h)}$ + [$d$(H-O) sin$\rho_{HO}$]}; [10] {$y_{O(a/h)}$ + $d$(Si-O)}; [11] {$y_{O(a/h)}$ + [(4/3) $d$(Si-O)]}.

Table 1B. Multiplicity and site symmetry in layer group: $c2/m$.

| Atom | Multiplicity | Site symmetry | Coordinates[1] |
|---|---|---|---|
| Al | 4 | *2* | (0, y, 0); (0, −y, 0) |
| $O_{apical}$ | 8 | *1* | (x, y, z); (−x, y, −z); (−x, −y, −z); (x, −y, z) |
| $O_{hydroxyl}$ | 4 | *m* | (x, 0, z); (−x, 0, −z) |
| H | 4 | *m* | (x, 0, z); (−x, 0, −z) |
| Si | 8 | *1* | (x, y, z); (−x, y, −z); (−x, −y, −z); (x, −y, z) |
| $O'_{basal}$ | 4 | *m* | (x, 0, z); (−x, 0, −z) |
| $O_{basal}$ | 8 | *1* | (x, y, z); (−x, y, −z); (−x, −y, −z); (x, −y, z) |

[1] (0, 0, 0)+, ($a/2$, $b/2$, 0)+.

1987; Davis and Kent, 1990; Parks, 1990). This instability drives the dissociative chemisorption of water molecules at Lewis acid sites at the exposed cut (Schindler and Stumm, 1987; Parks, 1990). Dissociative chemisorption of water molecules at the cut will be henceforth called healing.

A cut preserving stoichiometry leaves the surface charge-neutral. Healing, which changes the stoichiometry of the surface repeat unit by an integral number of water molecules, also leaves the surface charge-neutral. A pristine phyllosilicate edge face that has been cut and healed is at the point of zero net proton charge (PZNPC; Sposito, 1984).

### *Bulk pyrophyllite structure*

Table 1 contains the unit-cell coordinates of the single-layer pyrophyllite (layer group: c2/m) used in this study. Rather than use a crystal structure refinement from the literature, this model is useful because it formally satisfies the electrostatic valence principle (Pauling, 1929). Bond lengths were computed using the empirical equation and parameters of Brown and Shannon (1973).

Table 2. Estimated energies (Ziolkowski and Dziembaj, 1985) for cutting bonds to form selected pyrophyllite edge-faces. Repeat distance along {010} and {110} edge-faces is $a$. Repeat distance along {100} and {130} edge-faces is $b$.

| Edge-face | Bond type and number | | Total energy, nJ/m |
|---|---|---|---|
| | Si-O | Al-O | |
| {010} | 1 | 1 | 2.274 |
| {110} | 1 | 1 | 2.274 |
| {100} | 2 | 2 | 2.625 |
| {130} | 2 | 2 | 2.625 |

The point symmetry of Si- and Al-polyhedra are $\bar{4}3m$ (regular tetrahedron) and $\bar{3}m$ (trigonal anti-prism), respectively. The tetrahedral rotation angle $\alpha$ is 10°. Bond lengths in the idealized pyrophyllite compare favorably with those in the pyrophyllite-1Tc refinement of Lee and Guggenheim (1981): $d(\text{Si-O})_{1Tc,\,mean}$ = 1.62 ± 0.03 Å; $d(\text{Si-O})_{c2/m}$ = 1.625 Å; $d(\text{Al-O})_{1Tc,\,mean}$ = 1.91 ± 0.05 Å; $d(\text{Al-O})_{c2/m}$ = 1.909 Å. The unit cell parameters (a = 5.227 Å; b = 9.053 Å) are about 1% larger than in pyrophyllite-1Tc (Lee and Guggenheim, 1981; a = 5.160(2) Å; b = 8.966(3) Å). The orientation of the structural hydroxyl bond relative to the plane of the layer was taken to be 23.1° (Giese, 1979) and d(H-O) set equal to 0.864 Å. This H-O bond length corresponds to a bond valence of 1.0 valence unit (v.u.) (Brown and Shannon, 1973).

### *Pyrophyllite {010} and {110} edge faces*

Both pyrophyllite {010} and {110} heal by dissociatively adsorbing one-half water molecule per tetrahedral sheet and one per octahedral sheet, for a total of two water molecules per edge-face repeat unit. The proposed edge-face repeat unit composition of a cut and healed pyrophyllite {110} or {010} is: $[Al_4\{Si_8O_{19}(OH)_2\}(OH)_4(H_2O)]$. The pyrophyllite {110} edge face is represented schematically in Figure 2A and {010} in Figure 2B.

The energy per repeat unit required to cut the bonds and form either {010} or {110} edge faces appear in Table 2. Two bonds are cut per repeat unit, one Si-O bond (1.0 v.u.) and one Al-O bond (0.5 v.u.). The energies in Table 2 were computed using Eq. 1 and data from Ziolkowski and Dziembaj (1985).

A negatively charged site at either pyrophyllite {010} or {110} can result when a base removes a proton from the water molecule coordinating Al at the edge face, converting it into a hydroxyl ion. This is illustrated by Reaction 2.

$$[Al_4\{Si_8O_{19}(OH)_2\}(OH)_4(H_2O)]^0 + Na^+(aq) + OH^-(aq) = [Al_4\{Si_8O_{19}(OH)_2\}(OH)_5]^- + Na^+(aq) + H_2O \quad (2)$$

https://doi.org/10.1346/CCMN.1993.0410305 Published online by Cambridge University Press

Similarly, a positively charged site can be created when an acid adds a proton to the hydroxyl coordinating the Al, converting it into a water molecule. This is shown in Reaction 3.

$$[Al_4\{Si_8O_{19}(OH)_2\}(OH)_4(H_2O)]^0 + H^+ (aq) + Cl^- (aq) = [Al_4\{Si_8O_{19}(OH)_2\}(OH)_3(H_2O)_2]^+ + Cl^- (aq) + H_2O \quad (3)$$

The stereographic picture in Figure 3 schematically illustrates a mechanism for the hydrolysis of a phyllosilicate edge face. Similar illustrations could be imagined for the other edge faces. Figure 3 illustrates three pyrophyllite {010} repeat units, each in a different state of hydrolysis. The center repeat unit could represent a hypothetical state prior to hydrolysis, wherein a hydronium cation [$H_3O^+$] bridges two hydroxyl ions at the edge face.

$$[Al_4\{Si_8O_{19}(OH)_2\}(OH)_4(H_2O)]^0 + H_2O = [Al_4\{Si_8O_{19}(OH)_2\}(OH)_5(H_3O)]^0 \quad (4)$$

Reaction 2 can be modified using Reaction 4 to represent hydrolysis as the ion exchange of the adsorbed hydronium cation with a base cation. Reaction 5 would produce the state represented by the bottom repeat unit in Figure 3.

$$[Al_4\{Si_8O_{19}(OH)_2\}(OH)_5(H_3O)]^0 + Na^+ (aq) + OH^- (aq) = [Al_4\{Si_8O_{19}(OH)_2\}(OH)_5]^- + Na^+ (aq) + 2\,H_2O \quad (5)$$

Alternatively, the state pictured in the center repeat unit of Figure 3 could be viewed as a hydroxyl anion [$OH^-$] bridging two water molecules at the edge face (Reaction 6).

$$[Al_4\{Si_8O_{19}(OH)_2\}(OH)_4(H_2O)]^0 + H_2O = [Al_4\{Si_8O_{19}(OH)_2\}(OH)_4(H_2O)_2]^0 \quad (6)$$

By analogy with the example of Reaction 5, Reaction 3 can be modified using Reaction 6 to represent the ion exchange of the hydroxyl anion with an acid anion. Reaction 7 would produce the state represented by the top repeat unit in Figure 3 when an acid anion undergoes ion exchange with the adsorbed hydroxyl.

$$[Al_4\{Si_8O_{19}(OH)_2\}(OH)_4(H_2O)_2]^0 + H^+ (aq) + Cl^- (aq) = [Al_4\{Si_8O_{19}(OH)_2\}(OH)_3(H_2O)_2]^+ + Cl^- (aq) + H_2O \quad (7)$$

Figure 3, interpreted in Reactions 4–7, illustrates how hydrolysis can be viewed as an ion exchange reaction in which each edge-face repeat unit is a reactant. Depending on the proton affinity of the oxygens, the edge face at the PZNPC may consist almost exclusively of repeat units represented by the center cell in Figure 3 or it may consist of equal numbers of the repeat units represented by the top and bottom cells in Figure 3, the product of Reactions 5 and 7.

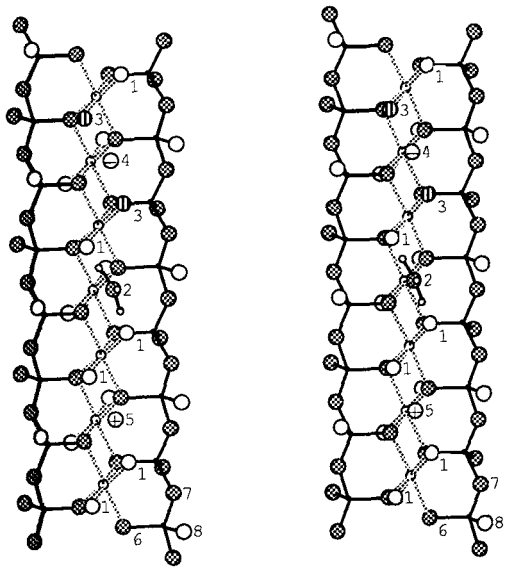

Figure 3. Stereographic illustration of a 2:1 phyllosilicate {010} edge face, viewed normal to the edge face with the layer oriented vertically in the page. Three edge-face repeat units appear in the illustration: an anion-exchange site (top), a neutral site (center), and a cation-exchange site (bottom). Numbers identify the following atoms: 1) hydroxyl oxygen of the octahedral layer, 2) hydronium [$H_3O^+$] cation, 3) water molecule, 4) exchangeable anion, 5) exchangeable cation, 6) apical oxygen linking tetrahedral and octahedral sheets, 7) oxygen at the basal plane of the tetrahedral sheet, and 8) silanol at the basal plane.

### *Pyrophyllite {100} and {130} edge faces*

The repeat distance along both {100} and {130} equals the b-dimension of the bulk unit cell ($3^{1/2}a$). Healing pyrophyllite {100} and {130} results in dissociative chemisorption of one water molecule per tetrahedral sheet and two per octahedral sheet, or a total of four water molecules per edge-face repeat unit. The proposed pyrophyllite {100} or {130} edge-face repeat unit composition following cutting and healing is: $[Al_5\{Si_{10}O_{23}(OH)_4\}(OH)_5(H_2O)_2]$. Unlike {010} and {110} edge faces, two protons per repeat unit can adsorb or desorb from octahedral oxygens at either the {100} or the {130] edge face.

Pyrophyllite {100} edge face may adopt one of two polymorphs. Polymorphic surfaces have identical compositions but different structures. The two edge-face polymorphs are designated $\alpha$ (Figure 4A) and $\beta$ (Figure 4B). Transferring a chain of silicate tetrahedra from the upper tetrahedral sheet in the $\alpha$-polymorph (Figure 4A) to the lower tetrahedral sheet converts it into the $\beta$-polymorph (Figure 4B). The relative positions of silanol groups and octahedral edge-face oxygens are clearly different in these two polymorphs.

The [110] periodic-bond-chain (PBC) (i.e., the A-chain in Figure 2A) and the [010] PBC (i.e., the B-chain in Figure 2B) are highlighted in Figure 5A, a

https://doi.org/10.1346/CCMN.1993.0410305 Published online by Cambridge University Press

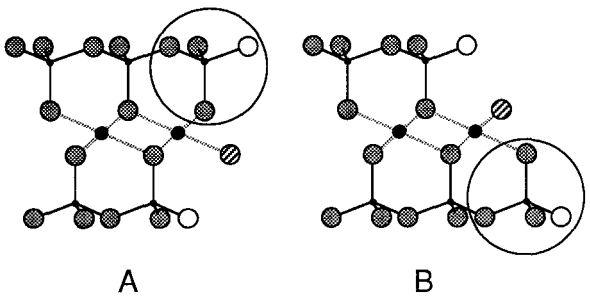


Figure 4. Profile illustrating the two polymorphs of 2:1 phyllosilicate {100} edge face: A) $\alpha$-polymorph and B) $\beta$-polymorph. The edge face is on the right-hand side in each illustration with the phyllosilicate layer extending to the left. Shaded circles denote oxygens, open circles are hydroxyls, and striped circles are water molecules. The large circle indicates the chain of tetrahedra whose position at the edge face distinguishes the A) $\alpha$-polymorph from the B) $\beta$-polymorph.

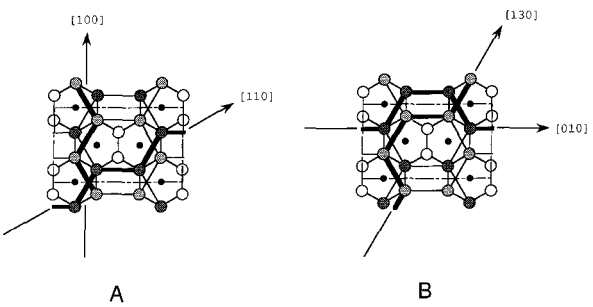


Figure 5. Illustration of a dioctahedral phyllosilicate unit cell with the octahedral sites appearing as hexagons (the {001} plane is in the plane of the page). Open circles indicate hydroxyl oxygens and filled circles denote apical oxygens of the tetrahedral sheets (the light and dark shading distinguishes the two tetrahedral sheets). Periodic Bond Chains (PBCs) consisting of chains of corner-sharing tetrahedra are indicated by heavy lines, the associated crystallographic directions [hk0] indicated by labeled arrows. The [100] and [110] PBCs (Figure 5A) border the {010} and {110} edge faces, respectively, and were identified by Grim and Guven (1978). The [010] and [130] PBCs (Figure 5B) border the {100} and {130} edge faces, respectively.

figure similar to that used by Grim and Guven (1978). These PBCs can be compared to the [010] and [130] PBCs highlighted in Figure 5B. The repeat distance along the [010] and [130] PBCs are the same, but the position of the edge face relative to the mirror plane passing through the hydroxyl ions is different. Figure 5B shows differences between pyrophyllite {100} and {130} edge faces that are not apparent from Figures 4A and 4B.

The energy per edge-face repeat unit required to cut the bonds and form {100} or {130} appears in Table 2. The bond-cutting energies for {100} and {130} are related to those for {010} and {110} by a factor of $(4/3)^{1/2}$, which accounts for the relative number of broken bonds and the relative repeat distances of the two types of edge faces.

### *Proton assignment and apparent valences of oxygens at pyrophyllite edge faces*

One strategy for assigning protons is to rank the reactivity of the edge-face oxygens by their unsaturated valency $\Delta\zeta_O$ (van Santen, 1982). The unsaturated valency $\Delta\zeta_O$ of oxygens is defined by Eq. 8.

$$\Sigma_i \{z_i/\nu_i\} - \zeta_{formal} = \Sigma_i \{s_i\} - 2 = \zeta_O - 2 = \Delta\zeta_O \quad (8)$$

The symbols in Eq. 8 represent cation formal charge ($z_i$), cation coordination number ($\nu_i$), oxygen formal charge ($\zeta_{formal} = 2$), bond valence ($s_i$) (Pauling, 1929) and apparent valence (O'Keeffe, 1989) or bond valence sum ($\zeta_O$). The sums in Eq. 8 are over all cations i directly bonded to the oxygen.

Basal oxygens $O_{basal}$ at the healed edge of tetrahedral sheets are bonded to one Si and one proton (O[H,Si]) instead of two Si atoms ($O[Si_2]$), as in the bulk. Replacing a Si-O bond with a H-O bond results in an unsaturated valency $\Delta\zeta_O$ of zero for the $O_{basal}$. Hydrolysis by adsorbing a proton ($O[H_2,Si]$; $\Delta\zeta_O = +1$ v.u.) or desorbing one (O[Si]; $\Delta\zeta_O = -1$ v.u) would require an extremely low or high pH.

The unsaturated valency $\Delta\zeta_O$ of octahedral oxygens at an edge face cannot be zero unless bond-length relaxation is permitted. The typical hydroxyl oxygen $O_{hydroxyl}$ at the healed edge of a dioctahedral sheet will be coordinated to one Al and one proton (O[Al,H]) resulting in an unsaturated valency $\Delta\zeta_O$ of $-\frac{1}{2}$ v.u. Charge neutrality at a healed pyrophyllite {010} at the PZNPC requires at least one water molecule coordinated to Al at the edge face.

The unsaturated valency $\Delta\zeta_O$ of an oxygen bonded to one Al and two protons ($O[Al,H_2]$) is $+\frac{1}{2}$ v.u. Similarly, protonated apical oxygens $O_{apical}$ (O[Al,H,Si]) at healed pyrophyllite {110}, {100} or {130} edge faces have an unsaturated valency $\Delta\zeta_O$ equal to $+\frac{1}{2}$ v.u. Healed pyrophyllite edge faces at the PZNPC, according to the simple crystallochemical model presented here, will always have one octahedral-sheet oxygen with an unsaturated valency $\Delta\zeta_O$ equal to $+\frac{1}{2}$ v.u. and a second with $\Delta\zeta_O$ equal to $-\frac{1}{2}$ v.u.

The two potentially over-/underbonded oxygens at the pyrophyllite {010} edge face are equivalent. However, the active-site oxygens at the pyrophyllite {110} edge face are not equivalent, resulting in two proton-assignment permutations: $O[Al,H_2]$ plus O[Al,Si]; or O[Al,H] plus O[Al,H,Si]. There are four active oxygens at both pyrophyllite {100} and {130}. Two O[H,Al] and two O[Si,Al] at pyrophyllite {100} permit three distinct proton-assignment permutations for each polymorph. Three O[H,Al], two in equivalent positions and a third in a unique position, and one O[Si,Al] at the pyrophyllite {130} allow four distinct proton-assignment permutations for each polymorph.

https://doi.org/10.1346/CCMN.1993.0410305 Published online by Cambridge University Press

## COMPUTATIONAL DETAILS

### *The one-dimensional lattice sum*

The electrostatic calculations in this paper assume atoms are dimensionless points charges. The charge assigned each atom equals its formal charge. With the exception of protons bonded to oxygens at the very edge of the layer (see below), the positions of all atoms remain fixed at their bulk unit-cell positions (Table 2).

Edge effects are modeled using the geometry illustrated in Figure 6. A single pyrophyllite layer is represented by a one-dimensional, infinite ribbon or lath with a finite width, W. Ribbon width W comprises an integral number n of bulk unit cells lying between two identical edge faces.

$$W = nd_{bulk} + 2d_{edge\ face} \quad (9)$$

The distance $d_{bulk}$ in Eq. 9 is the bulk repeat unit distance normal to the edge face, $d_{edge\ face}$ is the width of the surface repeat unit normal to the edge face, and n is an integer.

The ribbon has translational symmetry along its infinite z-axis, with repeat distance a. A one-dimensional lattice sum is appropriate for a periodic array of charge with this geometry. The one-dimensional lattice sum used to calculate the Coulomb potentials and energies in this paper was derived by Harris (1972, 1975) and improved by others (Andre *et al.*, 1978; Fripiat and Delhalle, 1979; Delhalle *et al.*, 1980). A complete discussion of the method is found in these references.

### *Optimizing OH bond-vectors at the edge face*

Giese (1976, 1979, and 1984) demonstrated the importance of hydroxyl-bond orientations in the stability of minerals. This paper uses optimized OH bond-vector orientations to allow for this effect on surface energy. The simplex optimization procedure described by Press *et al.* (1989) and used here, optimizes the orientation of all edge face OH bond-vectors simultaneously. The H-O-H bond angle of water molecules was set at 104.5° and all M-O-H bond angles (O coordinates a single M, M = Al or Si) were set at the tetrahedral angle (109.47°). In short, only the equatorial angle (the azimuthal angle being fixed) of each hydroxyl bond was optimized. The OH equatorial bond orientations were optimized against the total Coulomb energy of a pyrophyllite ribbon consisting of one bulk and two edge-face cells ($W = d_{bulk} + 2d_{edge\ face}$).

### *Reference potentials of protons and oxygens in ice*

Ice was chosen as the reference state for protons and oxygens adsorbed at the edge faces. The electrostatic self-potentials for protons and oxygens were computed using the Ewald (1921) lattice sum and coordinates reported by Leadbetter *et al.* (1985). The mean self-potential of the oxygens in ice IX is +31.72 volts. The mean self-potential of the protons is −20.74 volts.

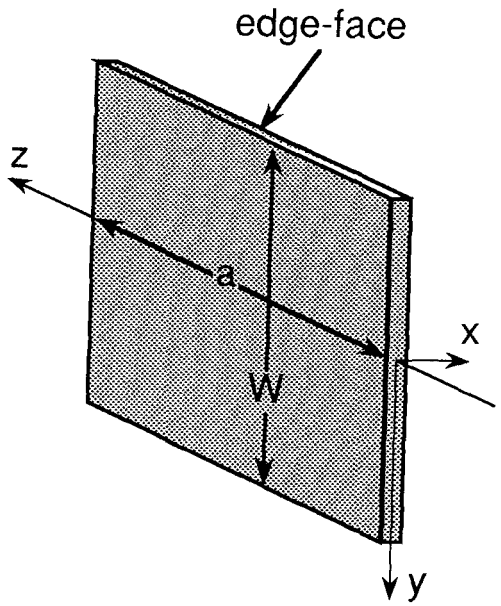


Figure 6. A schematic illustration of the one-dimensional, infinite ribbon used to simulate a phyllosilicate edge face for the purpose of computing Coulombic potentials with a one-dimensional lattice sum. The phyllosilicate consists of a single layer oriented so that the {001} crystallographic plane is in the xz-plane. The ribbon is periodic in the z-direction, with repeat distance a. The ribbon has infinite length in the z-direction, but finite width W in the y-direction, normal to the edge face. The width W counts two edge-face repeat units (width: $d_{edge\ face}$) and an integral number n of bulk repeat units (width: $d_{bulk}$). The integer n is varied until the potentials of ions in the center of the ribbon no longer change with increasing n.

## RESULTS AND DISCUSSION

### *OH bond-vector orientations at edge faces*

Stereographic illustrations of selected edge faces with optimized hydroxyl-bond orientations appear in Figures 7–10. There is usually more than one crystallochemically-equivalent way to assign protons to oxygens at an edge face. The proton assignments appearing in Figures 7–10 represent those assignments that yield the most negative surface Coulomb energies.

These OH bond-vector orientations (Figures 7–10) are appropriate for a point-charge model of healed edge faces in contact with a vacuum. The presence of fluid or solid water would certainly change OH bond-vector orientations from that pictured here. They do, however, provide some insight into the effective range of electrostatic interactions at the surface of a polar coordination compound.

Hydroxyl bonds orient under the influence of a local electrostatic potential. The orientations of silanol bonds are remarkably insensitive to alternative proton assignments at the octahedral edge-face oxygens, giving some indication of just how localized these electrostatic potentials actually are. The local structure of water at

https://doi.org/10.1346/CCMN.1993.0410305 Published online by Cambridge University Press

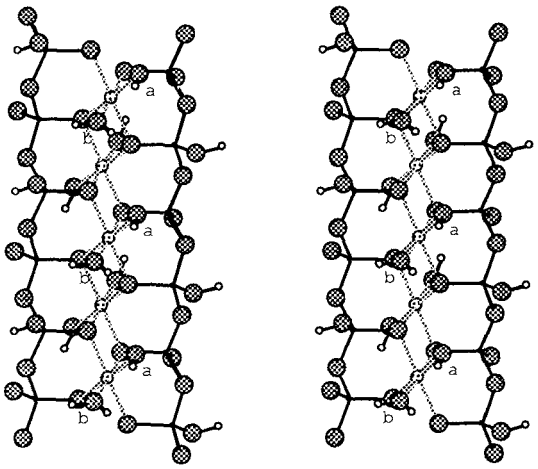

Figure 7. Stereographic illustration of the pyrophyllite {010} edge face showing optimized OH bond-vector orientations. Oxygens (shaded circles) labeled with letter (a) have an unsaturated valency $\Delta\zeta$ equal to $-\frac{1}{2}$ v.u.; those labeled with letter (b) have an unsaturated valency $\Delta\zeta$ equal to $+\frac{1}{2}$ v.u.; otherwise, their unsaturated valency $\Delta\zeta$ equals zero.

the edge face, itself responding to both the structure of bulk liquid water and the presence of a solid surface, will determine the actual hydroxyl-bond orientations in fully hydrated systems.

*Surface Coulomb potentials and energies at edge faces*

The surface Coulomb energy of clean-cut phyllosilicate edge faces are not representative of the surface Coulomb energies of healed edge faces. Healing has a profound and unexpected effect on the surface Coulomb energy, which goes beyond the obvious reduction in the unsaturated valency $\Delta\zeta_O$ of surface oxygens.

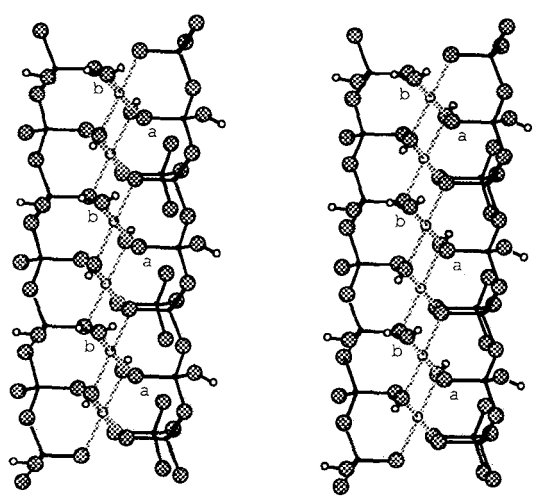

Figure 8. Stereographic illustration of the pyrophyllite {110} edge face showing optimized OH bond-vector orientations. Oxygens (shaded circles) labeled with letter (a) have an unsaturated valency $\Delta\zeta$ equal to $-\frac{1}{2}$ v.u.; those labeled with letter (b) have an unsaturated valency $\Delta\zeta$ equal to $+\frac{1}{2}$ v.u.; otherwise, their unsaturated valency $\Delta\zeta$ equals zero.

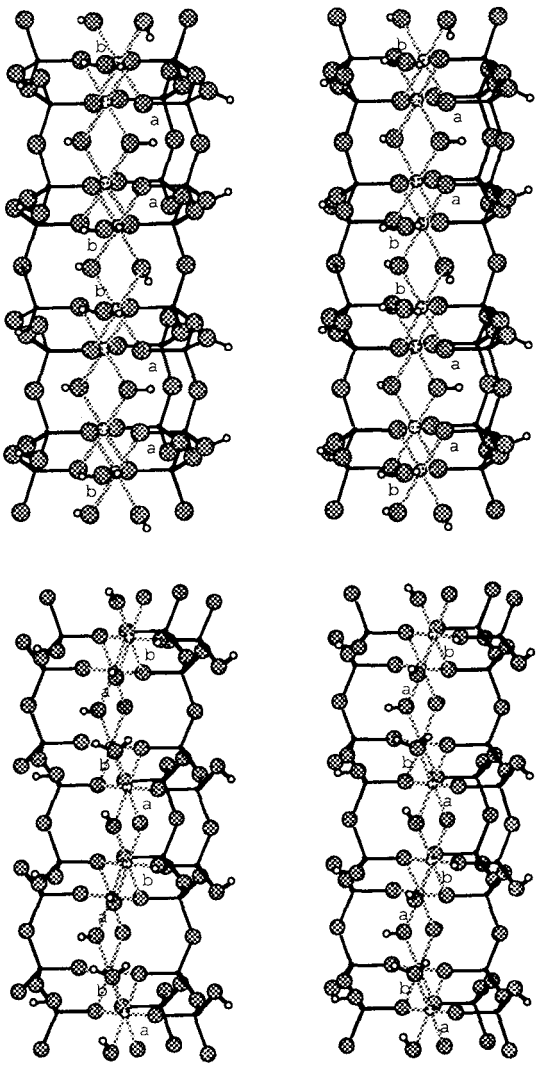

Figure 9. Stereographic illustration of two polymorphs of the pyrophyllite {100} edge face, showing optimized OH bond-vector orientations: A) $\alpha$-polymorph, and B) $\beta$-polymorph. Oxygens (shaded circles) labeled with letter (a) have an unsaturated valency $\Delta\zeta$ equal to $-\frac{1}{2}$ v.u.; those labeled with letter (b) have an unsaturated valency $\Delta\zeta$ equal to $+\frac{1}{2}$ v.u.; otherwise, their unsaturated valency $\Delta\zeta$ equals zero.

The surface Coulomb energy $\Gamma_{\text{Coulomb}}$ is computed from the self-potentials $\{\phi_i\}$ of the ions at and near the edge face relative to their self-potentials in the layer far from the edge face. The self potential $\phi_i$ is the Coulomb potential at an ion i due to all other ions in the system. This is expressed in Eq. 10.

$$\Gamma_{\text{Coulomb}} = (\frac{1}{2})[\Sigma_i q_i\{\phi^s{}_i - \phi^b{}_i\} + \Sigma_j q_j\{\phi^s{}_j - \phi^{ice}{}_j\}] \quad (10)$$

The first sum in Eq. 10 is over ions of the edge face whose self-potential at the surface $\phi^s{}_i$ is evaluated relative to its self-potential within the phyllosilicate layer

https://doi.org/10.1346/CCMN.1993.0410305 Published online by Cambridge University Press

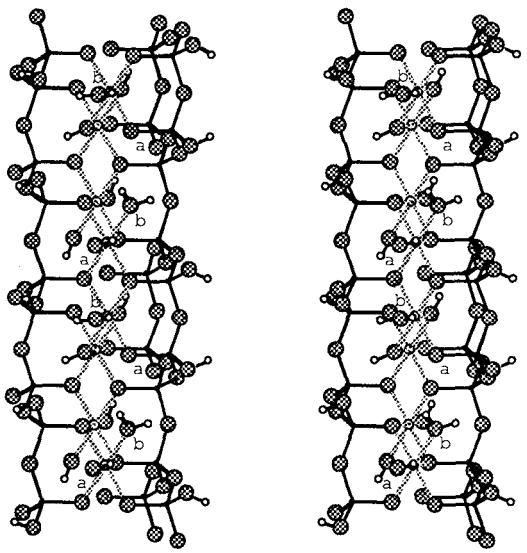

Figure 10. Stereographic illustration of the pyrophyllite {130} edge face, $\alpha$-polymorph. The $\beta$-polymorph is not illustrated. Oxygens (shaded circles) labeled with letter (a) have an unsaturated valency $\Delta\zeta$ equal to $-1/2$ v.u.; those labeled with letter (b) have an unsaturated valency $\Delta\zeta$ equal to $+1/2$ v.u.; otherwise, their unsaturated valency $\Delta\zeta$ equals zero.

Table 3. Surface-excess Coulomb energies of pyrophyllite edge-faces in the *PZNPC*-state. Repeat distance along {010} and {110} edge-faces is *a*. Repeat distance along {100} and {130} edge-faces is *b*.

| Edge-face | Proton assignment | Energy, nJ/m |
|---|---|---|
| {010} | 1. $O_{[Al,2H]}$; $O_{[Al,H]}$ | −1.794 |
| {110} | 2. $O_{[Al,2H]}$; $O_{[Al,Si]}$ | −2.296 |
| {110} | 3. $O_{[Al,H]}$; $O_{[Al,H,Si]}$ | −2.912 |
| $\alpha$-{100} | 4. $2O_{[Al,H]}$; $2O_{[Al,H,Si]}$ | −2.161 |
| $\alpha$-{100} | 5. $O_{[Al,2H]}$; $O_{[Al,Si]}$; $O_{[Al,H]}$; $O_{[Al,H,Si]}$ | −3.074 |
| $\alpha$-{100} | 6. $2O_{[Al,2H]}$; $2O_{[Al,Si]}$ | −3.488 |
| $\beta$-{100} | 7. $2O_{[Al,H]}$; $2O_{[Al,H,Si]}$ | −2.393 |
| $\beta$-{100} | 8. $O_{[Al,2H]}$; $O_{[Al,Si]}$; $O_{[Al,H]}$; $O_{[Al,H,Si]}$ | −3.583 |
| $\beta$-{100} | 9. $2O_{[Al,2H]}$; $2O_{[Al,Si]}$ | −3.402 |
| {130} | 10. $2O_{[Al,H]}$; $O'_{[Al,2H]}$; $O_{[Al,H,Si]}$ | −2.730 |
| {130} | 11. $O_{[Al,2H]}$; $O_{[Al,H]}$; $O'_{[Al,H]}$; $O_{[Al,H,Si]}$ | −2.881 |
| {130} | 12. $O_{[Al,2H]}$; $O_{[Al,H]}$; $O'_{[Al,2H]}$; $O_{[Al,Si]}$ | −3.639 |
| {130} | 13. $2O_{[Al,2H]}$; $O'_{[Al,H]}$; $O_{[Al,Si]}$ | −2.857 |

The cations coordinating each oxygen are listed in square brackets in the "Proton assignment" column. Water molecules may form by protonating a hydroxyl at three possible positions at the pyrophyllite {130} edge-face. The oxygen of one (inner) position at the {130} is marked with an apostrophe (O') in the "Proton assignment" column to distinguish it from the other two (outer) positions.

$\phi^b_i$, far from the edge face. The second sum is over the protons and oxygens of dissociatively chemisorbed water molecules whose self-potential at the surface $\phi^s_j$ is evaluated relative to their self-potential $\phi^{ice}_j$ in bulk ice. Ion charges are denoted as $q_i$.

The terms from Eq. 10 can be regrouped in Eq. 11 to yield two sums whose terms represent the individual ion contributions $q_i\Delta\phi_i/2$ to the surface Coulomb energy $\Gamma_{Coulomb}$.

$$\Gamma_{Coulomb} = [\Sigma_i\{q_i\Delta\phi^{layer}{}_i\}/2 + \Sigma_j\{q_j\Delta\phi^{sorbed}{}_j\}/2] \quad (11)$$

The first sum on the right-hand side of Eq. 11 is over the ions i of the phyllosilicate layer. The second sum in Eq. 11 is over the protons and oxygens j chemisorbed during healing. The choice of reference state for chemisorbed water molecules strongly influences the computed surface Coulomb energy.

The surface Coulomb energies $\Gamma_{Coulomb}$ for each possible proton assignment at the pyrophyllite {010}, {110}, {100} and {130} edge faces are listed in Table 3. The surface Coulomb energies $\Gamma_{Coulomb}$ range from −1.794 nJ/m to −3.639 nJ/m, indicating that healing via water chemisorption leads to a modest stabilization of these edge faces. Alternative proton assignments result in variations of the surface Coulomb energy covering a range of as much as 1.33 nJ/m.

Though certain proton assignments appear to be favored, variations of 1.33 nJ/m may not be significant compared to thermal energy. If this range is not physically significant, then the relative stability of one edge face over another may not be significant with the sole exception of the relatively modest instability of the {010} relative to the other edge faces listed in Table 3.

Pyrophyllite {100} and {130} edge faces adsorb twice as many water molecules per repeat unit than the {010} and {110} edge faces, yet the repeat distance of the former is 1.732 times the latter. This higher site density accounts for part of the stability that {100} and {130} edge faces exhibit relative to the {010} and {110}.

Figures 11A and 11B illustrate the variation in the surface Coulomb energy $\Gamma_{Coulomb}$ with distance from the edge face. This is done by plotting $q_i\Delta\phi_i$ for selected ions i as a function of repeat unit position. These figures quantify the range of the edge-face perturbation extending into the layer. Approximately 94 ± 3% of $\Gamma_{Coulomb}$ comes from ions in the edge-face repeat unit and another 4 ± 2% of $\Gamma_{Coulomb}$ from ions in the outermost bulk repeat unit. The initial decrease in $\Gamma_{Coulomb}$ with distance from the edge face into the layer is rapid, followed by a more gradual decrease that may extend to a depth of 25 to 35 repeat units (200 to 300 Angstroms) from the edge face.

Figures 11A and 11B illustrate another important phenomenon. Surface oxygen anions always destabilize $\Gamma_{Coulomb}$, while cations at the surface always stabilize $\Gamma_{Coulomb}$. Atomic charge $q_i$ and the magnitude of the self-potential $\phi_i$ are directly related. This is reflected in the magnitude of $q_i\Delta\phi_i$ for individual ions. Protons (Figure 11B) contribute much less to edge-face $\Gamma_{Coulomb}$ stabilization than, say, Si cations (Figure 11A).

The relative contributions of cations and anions to the surface Coulomb energy $\Gamma_{Coulomb}$ illustrated in Fig-

https://doi.org/10.1346/CCMN.1993.0410305 Published online by Cambridge University Press

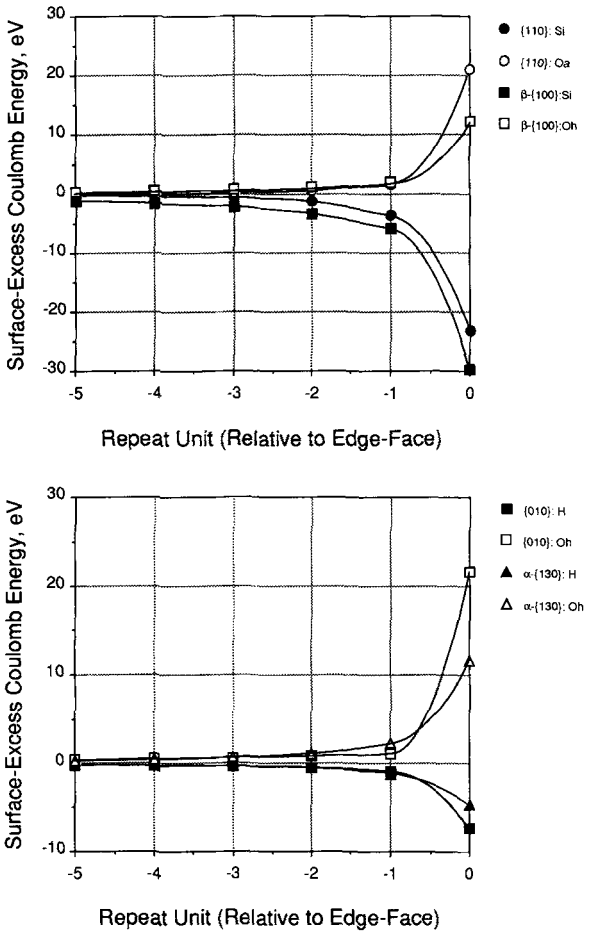


Figure 11. Surface-excess Madelung energy (electron volts) of selected ions as a function of repeat unit position: A) silicon and oxygen ions and B) protons and oxygen ions. The edge-face repeat unit is designated "0," while successive bulk repeat units are assigned negative numbers to indicate relative position. Symbol "Oh" indicates hydroxyl oxygens and "Oa" indicates apical oxygens.

ures 11A and 11B are a consequence of the healing of the edge face by the chemisorption of water. The self-potentials of both cations and anions at the cut edge face will be lower in magnitude relative to the bulk layer resulting in a positive $\Gamma_{Coulomb}$. This is because ions at the cut surface of a polar solid have fewer neighbors than bulk ions (Parry, 1975).

The situation is much different at the healed surfaces of polar coordination compounds where chemisorbed water restores the full coordination of surface cations. The healing of pyrophyllite edge faces results in a net stabilization of $q_{Al}\Delta\phi_{Al}$ and $q_{Si}\Delta\phi_{Si}$. Protons at the edge face also exhibit self-potentials that are usually more stable than in the bulk layer. This probably occurs because surface protons are involved in fewer repulsive cation-cation interactions at the edge face than in the bulk layer, where numerous $Al^{3+}$ and $Si^{4+}$ atoms occur in the second coordination sphere.

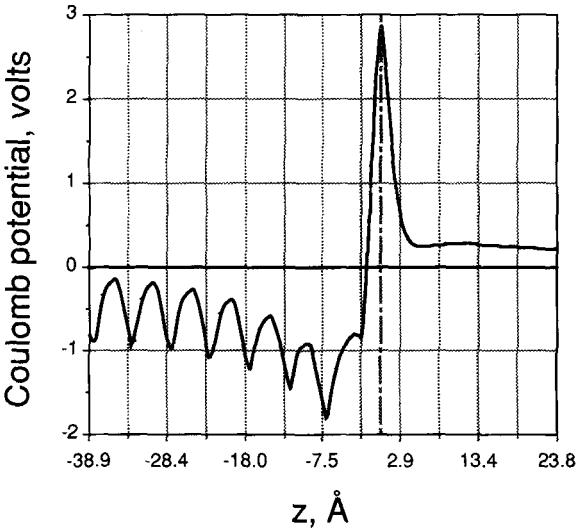


Figure 12. Coulombic potential of a test charge along a transect parallel to pyrophyllite {001} and normal to α-{100} (Figure 9A). Distance of test charge from the plane of basal oxygens equals 1.7957 Å. The plane of outermost basal oxygen atom is defined to be the origin, negative distance indicates positions above the pyrophyllite layer, while positive distance indicates positions beyond the edge face (the scale along the z-axis marks bulk unit cells). The edge face repeat unit extends from −7.538 Å to about the position of the dot-dashed line, which marks the position of the outermost silanol proton.

Oxygen self-potentials $\phi^{layer}{}_O$ are lower in magnitude at the edge face, yielding a positive $q_O\Delta\phi_O$ that destabilizes $\Gamma_{Coulomb}$. The self-potentials of edge-face cations are higher in magnitude, yielding a negative $q_i\Delta\phi_i$ that stabilizes $\Gamma_{Coulomb}$. This effect is reflected in the Coulomb potential along a transect parallel to the {001}, normal to the {hk0} edge face, and extending across the edge face to a region beyond the phyllosilicate layer (Figure 12).

Above the phyllosilicate layer, the Coulomb potential oscillates, the relative highs occur at the center of the ditrigonal ring and the relative lows occur above basal oxygens (Bleam, 1990). The oscillating Coulomb potential develops a gradual, negative trend as the edge face is approached, which parallels the trends exhibited by cations in Figures 11A and 11B. Immediately at the edge face, the Coulomb potential turns sharply positive and gradually returns to a zero potential far from the edge face. The sharp change from negative to positive Coulomb potentials results from silanol protons at the edge face (marked by the dot-dashed line) and the absence of oxygens.

### *Coulomb potentials of protons and ion-exchange sites at edge faces*

Van Santen (1982) proposed ranking the surface activity of protons and oxygens by their Coulomb potentials. Van Santen (1982) did not use a lattice sum

https://doi.org/10.1346/CCMN.1993.0410305 Published online by Cambridge University Press

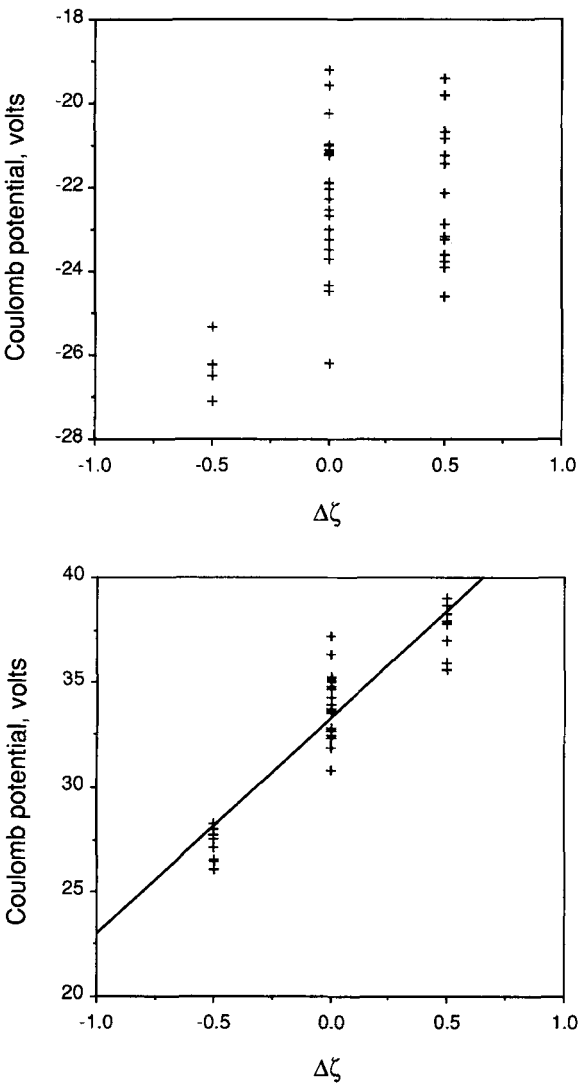


Figure 13. Coulombic potentials of A) protons and B) oxygens at the phyllosilicate edge faces illustrated in Figures 7–10, plotted against the oxygen unsaturated valency $\Delta\zeta_O$. The unsaturated valency $\Delta\zeta_O$ in B is the value assigned to the oxygen itself, while in A it is the value assigned to the oxygen to which the proton is bound. The line in B is the best fit linear model through the data points.

to compute Coulomb potentials, relying instead on the Evjen (1932) method. Glasser and Zucker (1980) and Coker (1983) have severely criticized the approximations Evjen (1932) used, casting some doubt on the results reported by van Santen (1982). The correlation between proton Coulomb potentials and other indicators of reactivity, such as oxygen coordination (Russell *et al.,* 1975) and the bond valence sum (Pauling, 1929; Hiemstra *et al.,* 1989), has never been examined.

Unsaturated valency $\Delta\zeta$ (Eq. 8) is a measure of the crystallochemical stability of the oxygen and, hence, the activity of the site. Some hydroxyl ions at the pyrophyllite {110}, {100}, and {130} edge faces are coordinated to two Al, just as in the bulk layer, yet the OH bond-vector reorients under the influence of the electrostatic field at the edge face. These structural hydroxyls have an unsaturated valency $\Delta\zeta_O$ equal to zero. Silanol oxygens at the edge faces also have unsaturated valencies $\Delta\zeta_O$ equal to zero.

From Figure 13A, we can see that the Coulomb potential of those protons bound to oxygens with an unsaturated valency $\Delta\zeta_O$ of $-\frac{1}{2}$ v.u. is more negative compared to protons bound to oxygens with an unsaturated valency $\Delta\zeta_O$ equal to zero and $+\frac{1}{2}$ v.u. There appears to be no difference between the Coulomb potentials of protons bound to oxygens with an unsaturated valency $\Delta\zeta_O$ equal to zero and those equal to $+\frac{1}{2}$ v.u.

Figure 13A demonstrates that the Coulomb potential of a proton is sensitive to a more extensive environment than is reflected by the immediate coordination of the oxygen to which it is bound. Differences in the proton environment induce a spread of proton potentials spanning 6 volts from $-19$ to $-25$ volts, a variation of about $\pm 15\%$. Proton Coulomb potentials are not reliable indicators of H-O bond strength because they are sensitive to longer range influences.

The correlation of surface-oxygen unsaturated valency $\Delta\zeta_O$ with the oxygen Coulomb potential is much better (Figure 13B) than with the proton Coulomb potentials (Figure 13A). Still, the range of Coulomb potentials experienced by oxygens whose unsaturated valency $\Delta\zeta_O$ equals zero overlaps markedly with oxygens with an unsaturated valency $\Delta\zeta_O$ equal to $+\frac{1}{2}$ v.u.

## CONCLUSIONS

The surface Coulomb energy is sensitive to OH bond-vector orientations; therefore, these bond vectors must be optimized to give a consistent estimate of the surface Coulomb energy. About 94% of the surface Coulomb energy arises in the edge-face repeat unit and another 4% in the outermost bulk repeat unit. In fact, the greatest contribution comes from the oxygens and protons at the edge face. Permutations in proton assignment to crystallochemically equivalent sites accounts for a 1.33 nJ/m variation in the surface Coulomb energy of a given edge face. This range is comparable to differences in the surface Coulomb energy between different edge faces.

The characteristics distinguishing {010} and {110} edge faces from {100} and {130} edge faces are these. The total bond energy needed to cut the pyrophyllite layer and form either {100} or {130} edge faces is about 16% higher (Table 2) than needed to form either {010} or {110}. This difference is small, but perhaps enough to account for the predominance of {010} and {110} edge faces over{100} and {130} in nature. A minimum of four water molecules must chemisorb per {100} or {130} surface repeat unit to heal those edge faces, com-

https://doi.org/10.1346/CCMN.1993.0410305 Published online by Cambridge University Press

pared with only two per {010} or {110} surface repeat unit. These extra water molecules effectively stabilize the surface Coulomb energy of the two former edge faces with the result that the surface Coulomb energies of the {110}, {100}, and {130} are equivalent. The {010} appears to be less stable than the other three edge faces (Table 3).

The surface Coulomb energies listed in Table 3 are for edge faces at the point of zero net proton charge. If the {010} and {110} edge faces were fully hydrolyzed through reactions such as 2 or 3, the maximum edge-face charge density would be 0.307 nC/m, compared with 5.04 nC/m at either the {100} or {130}. Relative edge-face stability may derive from the density of charge sites. The current study does not model hydrolysis and cannot compare the relative stability of charged edge faces.

Healing via dissociative chemisorption of water molecules results in a net stabilization of cation $q_i\Delta\phi_i$ energies, while oxygen $q_i\Delta\phi_i$ energies remain destabilized at the surface. The $q_i\Delta\phi_i$ energies of cations and anions are destabilized at the clean-cut surfaces of polar crystals because attractive interactions are lost from the first coordination sphere of both types of ions upon cutting. Healing restores the principal attractive interactions for the cations, but fails to do so for the outermost anions.

Proton Coulomb potentials show poor correlation with the unsaturated valency $\Delta\zeta_O$ of the oxygen to which it is bonded. Unsaturated valency $\Delta\zeta_O$ is an indicator of the immediate bonding environment, while Coulomb potentials respond to sufficient long-range interactions to obscure details of the local environment. The correlation between oxygen Coulomb potentials and their unsaturated valency $\Delta\zeta_O$ is somewhat better.

Finally, statistical mechanical simulations of ion and water interactions with smectite tactoids could employ the edge-face models and infinite-ribbon geometry used in this study. The simulation geometry would consist of one or more parallel smectite ribbons. The width of the ribbons could be chosen to eliminate edge effects at the ribbon center. These simulations could generate the positions of counter-ions, co-ions, water molecules, and surface OH bond-vector orientations using the edge-face models described in this study.

## ACKNOWLEDGMENTS

W. F. Bleam gratefully acknowledges the support both of the Cooperative States Research Service through Federal Hatch Grant No. 3289 and the Wisconsin Alumni Research Foundation through Grant No. 920284.

## REFERENCES

Andre, J. M., Fripiat, J. G., Demanet, C., Bredas, J. L., and Delhalle, J. (1978) Long-range Coulombic interactions in the theory of polymers: A statement of the problem and a method for calculation by the Fourier transformation method: *Int. J. Quantum Chem. Quantum Chem. Symp.* **12,** 233–247.

Bleam, W. F. (1990) The electrostatic potential at the basal {001} surface of talc and pyrophyllite as related to tetrahedral-sheet distortions: *Clays & Clay Minerals* **38,** 522–526.

Brown, I. D. and Shannon, R. D. (1973) Empirical bond-strength-bond-length curves for oxides: *Acta Cryst. A* **29,** 266–282.

Coker, H. (1983) Elementary methods for the evaluation of electrostatic potentials in ionic crystals: *J. Phys. Chem.* **87,** 2512–2525.

Davis, J. A. and Kent, D. B. (1990) Surface complexation modeling in aqueous geochemistry: *Rev. Mineral* **23,** 177–260.

Delhalle, J., Fripiat, J. G., and Piela, L. (1980) On the use of Laplace transform to evaluate one-dimensional lattice summations in quantum calculations of model polymers: *Int. J. Quantum Chem. Quantum Chem. Symp.* **14,** 431–442.

Evjen, H. M. (1932) On the stability of certain heteropolar crystals: *Phys. Rev.* **39,** 675–687.

Ewald, P. P. (1921) Die Berechnung optischer und elektrostatischer Gitterpotentiale: *Ann. Phys. (Leipzig)* **64,** 253–287.

Ferris, A. P. and Jepson, W. B. (1975) The exchange capacities of kaolinite and the preparation of homoionic clays: *J. Colloid Interface Sci.* **51,** 245–259.

Fripiat, J. G. and Delhalle, J. (1979) Fourier representation of the Coulombic contributions to polymer chains: *J. Comput. Phys.* **33,** 425–431.

Giese, R. F. (1976) Hydroxyl orientations in gibbsite and bayerite: *Acta Cryst. B* **32,** 1719–1723.

Giese, R. F. (1979) Hydroxyl orientations in 2:1 phyllosilicates: *Clay & Clay Minerals* **27,** 213–223.

Giese, R. F. (1984) Electrostatic energy models of micas: *Rev. Mineral* **13,** 105–144.

Glasser, M. L. and Zucker, I. J. (1980) Lattice sums: *Theoret. Chem. Adv. Perspect.* **5,** 67–139.

Grim, R. E. and Guven, N. (1978) *Bentonites: Geology, Mineralogy, Properties and Uses:* Elsevier, Amsterdam, 256 pp.

Harris, F. E. (1972) Fourier representation methods for electronic structures of linear polymers: *J. Chem. Phys.* **56,** 4422–4425.

Harris, F. E. (1975) Hartree-Fock studies of electronic structures of crystalline solids: *Theoret. Chem. Adv. Perspect.* **1,** 147–218.

Hartman, P. (1982) On the growth of dolomite and kaolinite crystals: *Neu. Jahr. Mineral. Monat.* **1982,** 84–92.

Hartman, P. and Perdok, W. G. (1955a) On the relations between structure and morphology of crystals. I: *Acta Cryst.* **8,** 49–52.

Hartman, P. and Perdok, W. G. (1955b) On the relations between structure and morphology of crystals. II: *Acta Cryst.* **8,** 521–524.

Hartman, P. and Perdok, W. G. (1955c) On the relations between structure and morphology of crystals. III: *Acta Cryst.* **8,** 524–529.

Hiemstra, T., van Riemsdijk, W. H., and Bolt, G. H. (1989) Multisite proton adsorption modeling at the solid/solution interface of (hydr)oxides: A new approach: *J. Colloid Interface Sci.* **133,** 91–104.

Leadbetter, A. J., Ward, R. C., Clark, J. W., Tucker, P. A., Matsuo, T., and Suga, H. (1985) The equilibrium low-temperature structure of ice: *J. Chem. Phys.* **82,** 424–428.

Lee, J. H. and Guggenheim, S. (1981) Single crystal x-ray refinement of pyrophyllite-1Tc: *Am. Mineral.* **66,** 350–357.

Muljadi, D., Posner, A. M., and Quirk, J. P. (1966) The mechanism of phosphate adsorption by kaolinite, gibbsite, and pseudoboehmite: *J. Soil Sci.* **17,** 230–237.

O'Keeffe, M. (1989) The prediction and interpretation of bond lengths in crystals: *Struct. bonding (Berlin)* **71,** 161–190.

O'Keeffe, M. and Stuart, J. A. (1983) Bond energies in solid oxides: *Inorg. Chem.* **22,** 177–179.

Parks, G. A. (1990) Surface energy and adsorption at mineral-water interfaces: An introduction: *Rev. Mineral* **23,** 133–175.

Parry, D. E. (1975) The electrostatic potential in the surface region of an ionic crystal: *Surface Sci.* **49,** 433–440.

Pauling, L. (1929) The principles determining the structure of complex ionic crystals: *J. Amer. Chem. Soc.* **51,** 1010–1026.

Press, W. H., Flannery, B. P., Teukolsky, S. A., and Vetterling, W. T. (1989) *Numerical Recipes in Pascal. The Art of Scientific Computing:* Cambridge, New York, 759 pp.

Quirk, J. P. (1960) Negative and positive adsorption of chloride by kaolinite: *Nature* **188,** 253–254.

Russell, J. D., Paterson, E., Fraser, A. R., and Farmer, V. C. (1975) Adsorption of carbon dioxide on goethite ($\alpha$-FeOOH) surfaces, and its implications for anion adsorption: *J. Chem. Soc., Faraday Trans. 1* **71,** 1623–1630.

Schindler, P. W. and Stumm, W. (1987) The surface chemistry oxides, hydroxides and oxide minerals: in *Aquatic Surface Chemistry,* W. Stumm, ed., Wiley, New York, 83–110.

Schofield, R. K. and Samson, H. R. (1953) The deflocculation of kaolinite suspensions and the accompanying change-over from positive to negative chloride adsorption: *Clay Mineral Bull.* **2,** 45–51.

Schofield, R. K. and Samson, H. R. (1954) Flocculation of kaolinite due to the attraction of oppositely charged crystal faces: *Disc. Faraday Soc.,* 135–145.

Secor, R. B. and Radke, C. J. (1985) Spillover of the diffuse double layer on montmorillonite particles: *J. Colloid Interface Sci.* **103,** 237–244.

Sposito, G. (1984) *The Surface Chemistry of Soils:* Oxford University Press, New York, 234 pp.

Sun, B. N. and Baronnet, A. (1989a) Hydrothermal growth of OH-phlogopite single crystals. I. Undoped growth medium: *J. Crystal Growth* **96,** 265–276.

Sun, B. N. and Baronnet, A. (1989b) Hydrothermal growth of OH-phlogopite single crystals. II. Role of Cr and Ti adsorption on crystal growth rater: *Chem. Geol.* **78,** 301–314.

Swartzen-Allen, S. L. and Matijevic, E. (1974) Surface and colloid chemistry of clays: *Chem. Rev.* **74,** 385–400.

Torrie, G. M. and Valleau, J. P. (1980) Electrical double layers. I. Monte Carlo study of a uniformly charged surface: *J. Chem. Phys.* **73,** 5807–5816.

Van Olphen, H. (1977) *An Introduction to Clay Colloid Chemistry,* 2nd ed.: Wiley, New York.

Van Santen, R. A. (1982) Chemical-bonding aspects of heterogeneous catalysis. II. Solid acids: *J. Roy. Neth. Chem. Soc.* **101,** 157–163.

White, G. N., and Zelazny, L. (1988) Analysis and implications of the edge structure of dioctahedral phyllosilicates: *Clays & Clay Minerals* **36,** 141–146.

Ziolkowski, J. (1986) Crystallochemical model of active sites on oxide catalysis: *J. Catal.* **100,** 45–58.

Ziolkowski, J., and Dziembaj, L. (1985) Empirical relationship between individual cation-oxygen bond-length and bond energy in crystals and in molecules: *J. Solid State Chem.* **57,** 291–299.

*(Received 3 September 1992; accepted 15 February 1993; Ms. 2271)*